ERDC/CRREL TR-19-8

Cold Regions Research and Engineering Laboratory

US Army Corps of Engineers®
Engineer Research and Development Center

ERDC
ENGINEER RESEARCH & DEVELOPMENT CENTER

ERDC 6.1 Basic Research

Measuring Very High Frequency and Ultrahigh Frequency Radio Noise in Urban Environments

A Mobile Measurement System for Radio-Frequency Noise

Caitlin E. Haedrich and Daniel J. Breton

June 2019




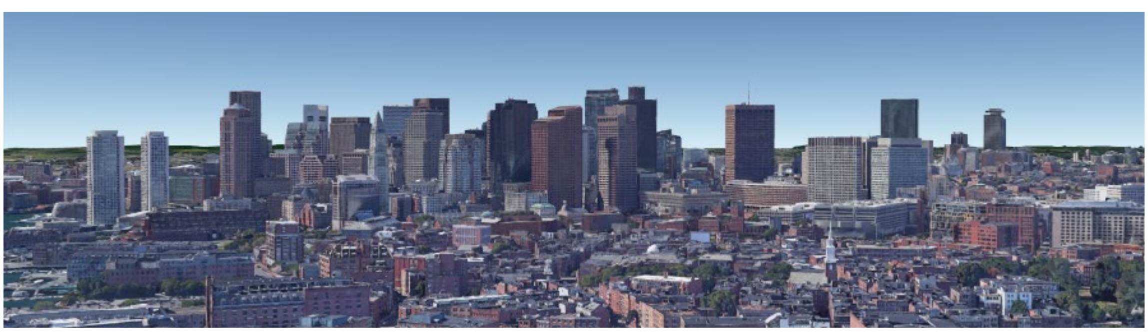

ERDC 6.1 Basic Research

ERDC/CRREL TR-19-8
June 2019

Measuring Very High Frequency and Ultrahigh Frequency Radio Noise in Urban Environments

A Mobile Measurement System for Radio-Frequency Noise

Caitlin E. Haedrich and Daniel J. Breton

U.S. Army Engineer Research and Development Center (ERDC)
Cold Regions Research and Engineering Laboratory (CRREL)
72 Lyme Road
Hanover, NH 03755-1290

Final Report

Prepared for Headquarters, U.S. Army Corps of Engineers
Washington, DC 20314-1000

Under ERDC 6.1 Basic Research, Project 61110252C00, “Geography of RF and Acoustic Urban Noise”

Abstract

Radio-frequency (RF) background noise is an important parameter in designing and predicting performance of RF communication and sensor systems. Modern man-made RF noise consists of unintentional emissions from sources such as electronic devices, power transmission lines, and internal combustion engine ignitions. Governments and academia have previously measured RF noise at fixed, representative locations within the urban environment. Considering the heterogeneous mix of office buildings, retail and residential buildings, transportation hubs, and parks that compromise modern cities, we hypothesize that RF-noise power varies significantly throughout the urban environment.

To characterize this variability, we present a mobile, tunable RF-noise measurement system designed to record frequencies from 63 MHz to 1 GHz in a 1 MHz to 10 MHz bandwidth. This report describes the system design, including the choice of preselection filters, preamplifiers, and RF shielding necessary to measure low RF-noise levels while avoiding intermodulation distortion problems that arise in an environment with many strong emitters. Additionally, we describe techniques developed to reliably geolocate RF data in urban environments. GPS (global positioning system) reception is often poor in dense urban environments. We mitigate this issue by using a 1 m surveying wheel for geolocation.

Contents

Abstract ii

Figures and Tables iv

Preface vi

Acronyms and Abbreviations vii

1 Introduction 1

1.1 Background 1
1.2 Objectives 2
1.3 Approach 2

2 System Design 3

2.1 Noise measurement theory 3
2.2 Determining internal noise 4
2.3 System hardware and sensitivity 5
2.4 Geolocation methods 8

3 Measurement Methods 10

3.1 Survey area 10
3.2 Spectrum survey 11

4 Results 12

4.1 Median external noise power 12
4.2 Peak power 17
4.3 Temporal noise-power variability 21

5 Discussion 23

5.1 Temporal variability in noise power 23
5.2 Spatial variability in noise power 23
5.3 Comparison to the ITU model and previous studies 25

6 Conclusion 27

References 28

Appendix A: Noise Figures and Y-Factor Method 30

Appendix B: Geolocation with Survey Wheel Code 33

Appendix C: Geolocation Code for GPS 35

Report Documentation Page

Figures and Tables

Figures

1 Schema of the mobile noise measurement system 5
2 Mobile Noise Measurement System deployed in Boston with labeled components 7
3 Trigger circuit for the measuring wheel and RF recorder 9
4 Map of the survey area and route through downtown Boston, Massachusetts. The route is 2.14 km long 10
5 Map of the survey area and route through the North End of Boston, Massachusetts. The route is 2.32 km long 11
6 Median external noise power in Boston's downtown (*top*) on 24 October and North End (*bottom*) on 10 October 2018 at 142 MHz. The second lap is shifted to be displayed alongside the first lap; the route walked was the same as the first lap. Areas labeled by A, B, and C are referenced in Fig. 17. Values below −97.8 dBm are too close to the system noise floor to be reliable 13
7 Median external noise power in Boston's downtown (*top*) on 9 October and North End (*bottom*) on 10 October 2018 at 246.5 MHz. The second lap is shifted to be displayed alongside the first lap; the route walked was the same as first lap 14
8 Median external noise power in Boston's downtown (*top*) on 9 October and North End (*bottom*) on 10 October 2018 at 972 MHz. The second lap is shifted to be displayed alongside the first lap; the route walked was the same as first lap. Values below −110.7 dBm are too close to the system noise floor to be reliable 15
9 Histograms of median external noise power at 142 MHz for samples collected every meter throughout the North End (*bottom*) and downtown Boston (*top*) on 10 and 24 October, respectively. The *dashed line* is the minimum system sensitivity, 0.75 dB above the system noise 16
10 Histograms of median external noise power at 246.5 MHz for samples collected every meter throughout downtown Boston (*top*) and the North End (*bottom*) on 9 and 10 October, respectively. The *dashed line* is the minimum system sensitivity, 0.75 dB above the system noise 16
11 Histograms of median external noise power at 972 MHz for samples collected every meter throughout downtown Boston (*top*) and the North End (*bottom*) on 9 and 10 October, respectively. The *dashed line* is the minimum system sensitivity, 0.75 dB above the system noise 17
12 Peak noise power at 142 MHz in downtown Boston (*top*) on 24 October and the North End (*bottom*) on 10 October. Letters are referenced in Fig. 17 18
13 Peak noise power at 246.5 MHz in downtown Boston (*top*) on 9 October and the North End (*bottom*) on 10 October 19
14 Peak noise power at 972 MHz in downtown Boston (*top*) on 9 October and the North End (*bottom*) on 10 October 20
15 Median noise power varying with distance along the route in Boston's downtown (*top*) and North End (*bottom*). Power levels are consistent between laps completed an hour apart 22

16 Median noise-power levels in downtown Boston from surveys taken 2 weeks apart at 142 MHz. Power levels are generally consistent between weeks 22

17 Median power and peak power (0.01%) at 142 MHz in Boston's North End shows the presence of impulsive noise. Points in regions A and B are dominated by Gaussian noise. Points in region C have strong impulsive components. The cluster of points at −54 dBm is at the maximum system sensitivity 24

Tables

1 Components of the mobile noise measurement system 6

2 Signal Hound BB60 Spectrum Analyzer / RF Recorder settings 6

3 Sensitivity characteristics of the mobile noise measurement system and its components calculated using the Y-factor method and from the user manuals (for maximum measurable power) 8

4 Date and time of noise surveys. Times reported are start times; the laps take about an hour 21

5 Comparison of median external noise values 26

A-1 Y-factor method measurements. The reported powers are the average over a 1-minute recording 30

A-2 Excess-noise ratio (ENR) of the Fairview Microwave Calibrated Noise Source 31

A-3 RF recorder and total system noise figure calculations 32

A-4 Component noise figure calculations 32

Preface

This study was conducted for the U.S. Army Corps of Engineers, using Military Direct Funds, under Engineer Research and Development Center (ERDC) 6.1 Basic Research Project 61110252C00, "Geography of RF and Acoustic Urban Noise." The technical monitor was Dr. Marino A. Niccolai, ERDC Cold Regions Research and Engineering Laboratory (CRREL).

The work was performed by the Signature Physics Branch (CEERD-RRD) of the Research and Engineering Division (CEERD-RR), ERDC-CRREL. At the time of publication, Dr. Marino A. Niccolai was Chief, CEERD-RRD; and Mr. Jared Oren was Acting Chief, CEERD-RR. The Deputy Director of ERDC-CRREL was Mr. David B. Ringelberg, and the Director was Dr. Joseph L. Corriveau.

COL Ivan P. Beckman was Commander of ERDC, and Dr. David W. Pittman was the Director.

Acronyms and Abbreviations

CRREL	Cold Regions Research and Engineering Laboratory
ENR	Excess-Noise Ratio
ERDC	U.S. Army Engineer Research and Development Center
GPS	Global Positioning System
HF	High Frequency
IFBW	Intermediate Frequency Bandwidth
I/Q	In-Phase and Quadrature
ITU	International Telecommunications Union
LiPo	Lithium Polymer
NMEA	National Marine Electronics Association
RF	Radio Frequency
SNR	Signal-to-Noise Ratio
UHF	Ultrahigh Frequency
VHF	Very High Frequency

1 Introduction

1.1 Background

Radio-frequency (RF) background noise is a spatially varying and critical parameter for predicting radio communication and electromagnetic sensor system performance in urban environments. High levels of RF noise can degrade RF system performance by decreasing intelligibility, increasing bit-error rates, and decreasing sensitivity in analog, digital, and sensing systems, respectively. Therefore, accurate measurements of noise power and its variability throughout the urban environment are crucial to support military and first-responder operations. The U.S. Army Corps of Engineers and the Cold Regions Research and Engineering Laboratory (CRREL) in Hanover, New Hampshire, recognizes that a greater understanding of noise variability will support military radio operations in urban areas.

RF noise comes from many different sources, both man-made and natural. Natural noise, such as galactic and atmospheric sources, are most powerful in the high-frequency (HF) range (3–30 MHz) and decrease in power through the low very high frequency (VHF) range (30–300 MHz) (ITU [International Telecommunications Union] 2016). At frequencies typically used for line-of-sight communications by military and first responders in the high VHF to ultrahigh frequency (UHF) range (300–3000 MHz), natural noise is low in power (ITU 2016) and is typically dominated by man-made noise, even in rural settings (Leferink et al. 2010).

Modern man-made RF noise consists of unintentional emissions from sources such as electronic devices, power transmission lines, and internal combustion engine ignitions (ITU 2016). Electronic devices such as cellular phones, wireless internet routers, laser printers, and photocopiers, in particular, are relevant to the urban noise environment because of their increasing pervasiveness in urban environments over the last decade.

Our early understanding of urban man-made noise was developed in the 1970s. Spaulding and Disney (1974) conducted a large-scale survey of noise, including urban, rural, and residential measurements taken in North America, Europe, and Asia. Their study provided the foundational dataset for Recommendation ITU-R P.372, *Radio Noise* (ITU 2016), a widely used model for predicting RF-noise power. ITU-R P.372 assumes that noise power centered at a given frequency between 0.3 to 250 MHz has a Gaussian distribution when expressed in decibels, a model first presented by Hagn and Sailors (1979). Hagn and Sailors (1979) also discuss a simple model for variations in noise power based on frequency.

Since the 1970s, substantial efforts have been made to update and expand the surveys of Spaulding and Disney (1974). Achatz and Dalke (2001) conducted a noise-power survey at 137 MHz and 402.5 MHz in Denver and Boulder, Colorado. Wagstaff and Merricks (2005) conducted in the UK a similar study to Disney and Spalding (1974). Most recently, Wepman and Sanders (2011) conducted measurements at 112.5 MHz, 221.5 MHz, and 401 MHz around the greater Denver area. Achatz and Dalke (2001), Wagstaff and Merricks (2005), and Wepman and Sanders (2011) each constructed noise measurement facilities housed in vans that were dispatched to different stationary (fixed) sites where they collected noise measurements. Wagstaff and Merrick's (2005) results, in particular, indicate that the background RF noise may have changed significantly since the Spaulding and Disney (1974) study with changing electronic device technology and usage. None of these studies characterized spatial variation in noise power.

1.2 Objectives

This study aims to address the lack of spatial discrimination in previous work by developing and deploying a mobile noise measurement system. This report provides an overview of the mobile measurement system and presents results collected in Boston, Massachusetts, in October 2018.

1.3 Approach

We developed and deployed a mobile, calibrated, and tunable (63 MHz to 1 GHz) RF-noise measurement system, utilizing a 1 m survey wheel to locate measurements in space. Our measurement system measures the modern urban noise field at ground level and characterizes spatial variability of urban RF noise. We deployed our system in Boston, Massachusetts, as a proof of concept and show that there is significant spatial variability in noise power throughout both the downtown and a neighboring residential area.

2 System Design

2.1 Noise measurement theory

The relationship between a transmitted signal and a measured signal at a receiver can be summarized by a link budget, shown in equation (1) (Norton 1953). Although link budgets are typically used for receive-transmit systems, we use the budget as a starting point to describe noise measurement systems. In this section, we follow the common practice of using capital letters to denote variables in decibels and their lowercase partners for the corresponding linear value.

$$P_0 + L_t + G_t = \mathrm{R} + L_b(d_0) + G_r + L_r + F_n + B + 10log_{10}(kT), \quad (1)$$

where

P_o = the transmission power of the signal (dBm);
L_t = the insertion loss of the transmitting system components, such as cables (dB);
G_t = the transmitting antenna gain (dBi);
R = the minimum signal-to-noise ratio (SNR) for satisfactory reception (dB);
$L_b(d_o)$ = the transmission loss over range d_o (dB);
G_r = the receiving antenna gain (dBi);
L_r = the insertion loss of the receiving system components (dB);
F_n = the total system noise figure measured in decibels relative to thermal noise (dB);
B = the receiver noise bandwidth (dB);
k = Boltzmann's constant, 1.38×10^{-23} J K^{-1}; and
T = the receiver temperature, typically assumed to be 290 K.

Without an intentionally transmitted signal, we simplify Equation (1) by removing the variables that concern the transmitted signal and transmitting system (P_o, L_t, and G_t). We also set the path loss and insertion loss in the receiving system ($L_b(d_o)$ and L_r) equal to zero. For the purposes of this discussion, the receiving antenna gain (G_r) is assumed to be isotropic and equal to zero. Lastly, since we are measuring noise, our SNR, R, is also zero (in linear units, it is 1: the received noise over received noise). Thus, the remaining variables describe the measured noise power, denoted P_n:

$$P_n = F_n + B + 10log_{10}(kT). \quad (2)$$

Moving from decibels to linear units, this equation becomes

$$p_n = f_n kTb. \tag{3}$$

The total noise factor, f_n, can be further broken down into internal and external factors (Norton 1953) where internal factors result from receiving system noise only:

$$f_n = f_a + l_c l_t f_r - 1, \tag{4}$$

where

f_n = the total noise factor,
f_a = the received external noise factor where $f_a = \frac{p_a}{kTb}$ and p_a is the total external received noise power,
l_c = the loss factor for the receiving antenna circuit,
l_t = the loss factor of the transmission cable connecting the antenna and receiver, and
f_r = the receiver system internal noise factor.

We are interested in f_a, the total external noise received by the antenna (man-made noise, natural noise, and intentional emitters). Solving for f_a yields

$$f_a = f_n - l_c l_t f_r + 1. \tag{5}$$

If we further assume the antenna circuit and cables are lossless, we can simplify Equation (5) to

$$f_a = f_n - f_r + 1. \tag{6}$$

Substituting Equation (3) into Equation (6), we relate total measured noise power (p_n) to receiving antenna external noise factor (f_a):

$$f_a = \frac{p_n}{kTb} - f_r + 1. \tag{7}$$

2.2 Determining internal noise

As shown in equation (7), the receiver's internal noise factor, f_r, is required to determine the external noise. We use the Y-factor method (also referred to as noise diode calibration) described by Hess (1998) and Keysight Technologies (2018). This method relies on having a noise source with a known excess-noise ratio (ENR) and has two steps: a calibration measurement with the noise source and RF recorder and a measurement with another system component such as a preamplifier inserted between the RF recorder and the noise source.

Significant amounts of time are required to complete the Y-factor method. Therefore, we performed this technique only once per frequency in a laboratory setting. The results are discussed in the "System hardware and sensitivity" section. Appendix A presents the procedure and calculations. In the field, the internal noise factor, f_r, is measured using a 50-ohm terminator to ensure that our setup is correct and to account for variations in internal noise that may occur between measurement sites.

2.3 System hardware and sensitivity

The measurement system, shown schematically in Figure 1 with system specifications listed in Table 1, is controlled using a ruggedized laptop computer with a solid-state drive to allow for fast writing speeds.

Figure 1. Schema of the mobile noise measurement system.

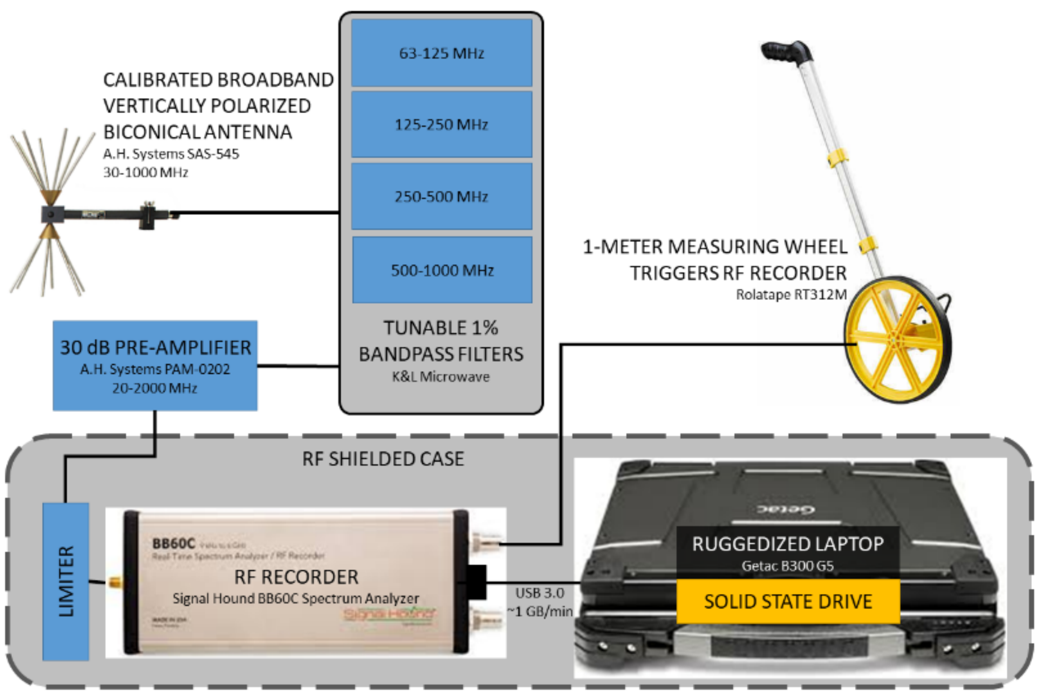

Table 1. Components of the mobile noise measurement system.

Device	Brand and Model
1 m Measuring Wheel	Rolatape RT312M
GPS (global positioning system)	GlobalSat BU-353S4
Antenna	A.H. Systems, Inc., SAS-545 Biconical Antenna (30 MHz–1 GHz)
Preamplifier	A.H. Systems, Inc., PAM-0202 30dB Preamplifier
Tunable 1% Bandpass Filters	K&L Microwave 5BT-500/1000-1-N/N K&L Microwave 5BT-250/500-1-N/N K&L Microwave 5BT-125/250-1-N/N K&L Microwave 5BT-63/125-1-N/N
Limiter	Mini Circuits VLM-63-2W-S+
Spectrum Analyzer	Signal Hound BB60C Spectrum Analyzer / RF Recorder
Laptop Computer	Getac B300 G5

The laptop records data collected by a Signal Hound BB60C Spectrum Analyzer / RF recorder. The spectrum analyzer, when operating in zero-span mode, has the capability to function as an RF recorder and to record in-phase and quadrature (I/Q) data in a 1 MHz bandwidth, resulting in a sample rate of 1.25×10^6 Hz. Table 2 provides a full list of RF recorder settings. A limiter protects the spectrum analyzer front end from signals powerful enough to cause damage. The laptop and RF recorder are housed in an RF-shielded case; our laboratory measurements show that the ruggedized laptop can contribute more than 10 dB of noise at frequencies above 500 MHz. The RF-shielded case, preamplifier, and filter are housed on wood shelves that are mounted on a frame backpack (Figure 2).

Table 2. Signal Hound BB60 Spectrum Analyzer / RF Recorder settings.

Field	Setting
Input Power/Reference Level	−40 dBm
Decimation	32
IFBW (Intermediate Frequency Bandwidth)	1 MHz
Auto IFBW	On
Sweep Time	1.00 ms
Trigger Type	External Trigger
Trigger Edge	Rising Edge
Trigger Level	0 dBm
Trigger Position	10.00%
Auto Spectrum	On
Pre-Trigger (Samples)	1024
Capture Size	250 ms
Max Number of Files	10,000

Figure 2. Mobile Noise Measurement System deployed in Boston with labeled components.

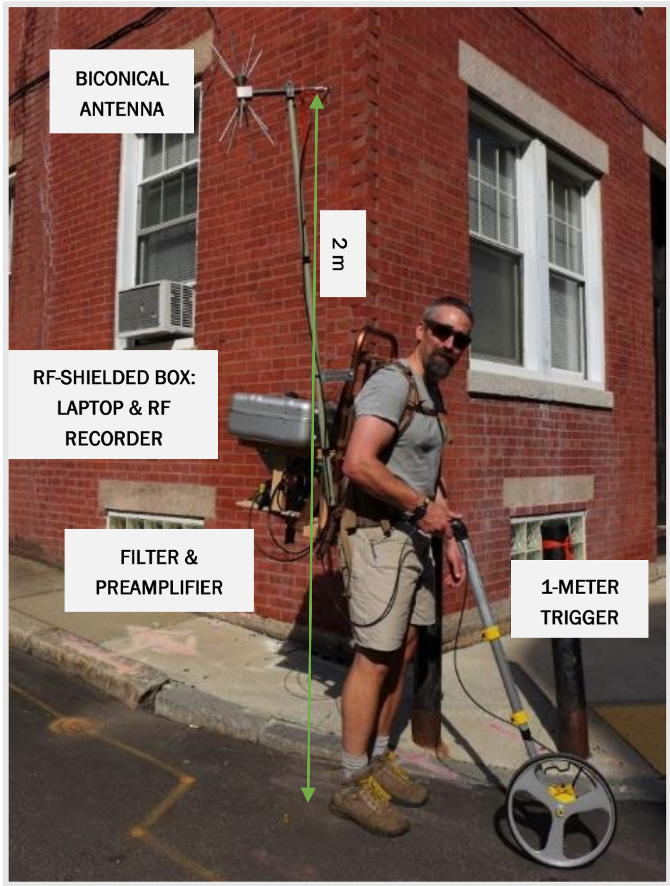

A bank of tunable bandpass filters is used for preselection. Like most spectrum analyzers, the Signal Hound BB60C has no internal preselection filtering capability, implying that all RF power collected by the antenna (including very strong emitters and low-level noise) reaches the RF front end of the spectrum analyzer. Failing to use preselection filters to exclude intentional emitters often leads to significant overload of the spectrum analyzer front end, resulting in intermodulation distortion and other spurious signals contaminating the measured noise power. Although the noise figures of tunable filters are higher than static ones, we opt for tunable because they give more flexibility in the field where one may not know a priori which frequencies will be free of emitters. Switching between the filters is done manually, disconnecting the system and antenna and reconnecting to the desired filter.

The 30 dB preamplifier is critical to the system as it lowers the overall system noise figure (F_r) to approximately the noise figure of the preamplifier, as discussed in Seybold (2005). Table 3 provides the components and total system noise figures along with the minimum and maximum measurable signal (system sensitivity).

Table 3. Sensitivity characteristics of the mobile noise measurement system and its components calculated using the Y-factor method and from the user manuals (for maximum measurable power).

Component	Frequency (MHz)	Noise Figure (dB)	Gain (dB)	Minimum Detectable Signal (dBm)	Maximum Measurable Power (dBm)
Signal Hound BB60C	142	18.28			
	246.5	18.25			
	972	18.67			
Preamplifier	142	3.78	30.80		
	246.5	3.99	30.56		
	972	4.15	29.84		
Tunable Bandpass Filter 125–250 MHz	142	2.3	−4.18		
	246.5	1.75	−2.27		
Tunable Bandpass Filter 500–1000 MHz	972	1.23	−1.54		
A.H. System, Inc., SAS-545 Biconical Antenna	142		−9.28		
	246.5		2.73		
	972		1.37		
Total System	142	7.55	17.80	−106.45	−52.3
	246.5	6.64	30.68	−107.36	−65.2
	972	5.15	30.62	−108.85	−64.9

2.4 Geolocation methods

The measurement system can be configured to use either GPS (global positioning system) or a measuring wheel for geolocation. In dense urban environments, tall buildings scatter GPS signals, preventing reliable geolocation. Where this occurs, the measuring wheel offers an effective alternative. The RF recorder records data when triggered by a 1 m circumference measuring wheel. With each complete rotation, a reed switch sends a signal to the RF recorder, which collects a 250 ms recording (312,500 samples) at a user-set frequency and bandwidth. The reed switch closes the circuit when a magnet mounted on the wheel passes the switch, sending a signal to the RF recorder's trigger port (Figure 3). The circuit uses a 3.7 V rechargeable lithium polymer (LiPo) battery.

The wheel is walked in a straight line along a city block, stopping at each block corner to record the number of meters walked along the straightaway. The length in meters of the sidewalk and the number of files recorded are the same. The location of each file is interpolated between each corner. Appendix B provides the methods and code for this interpolation.

Figure 3. Trigger circuit for the measuring wheel and RF recorder.

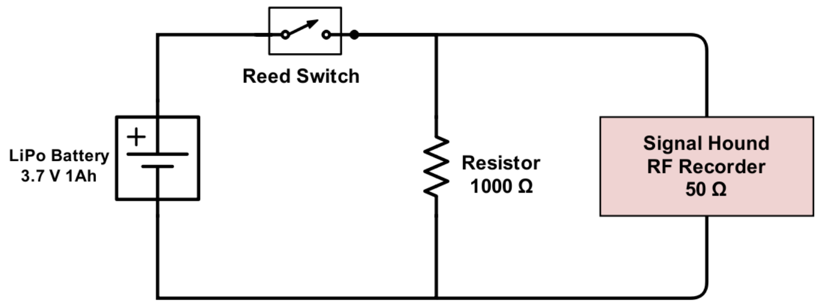

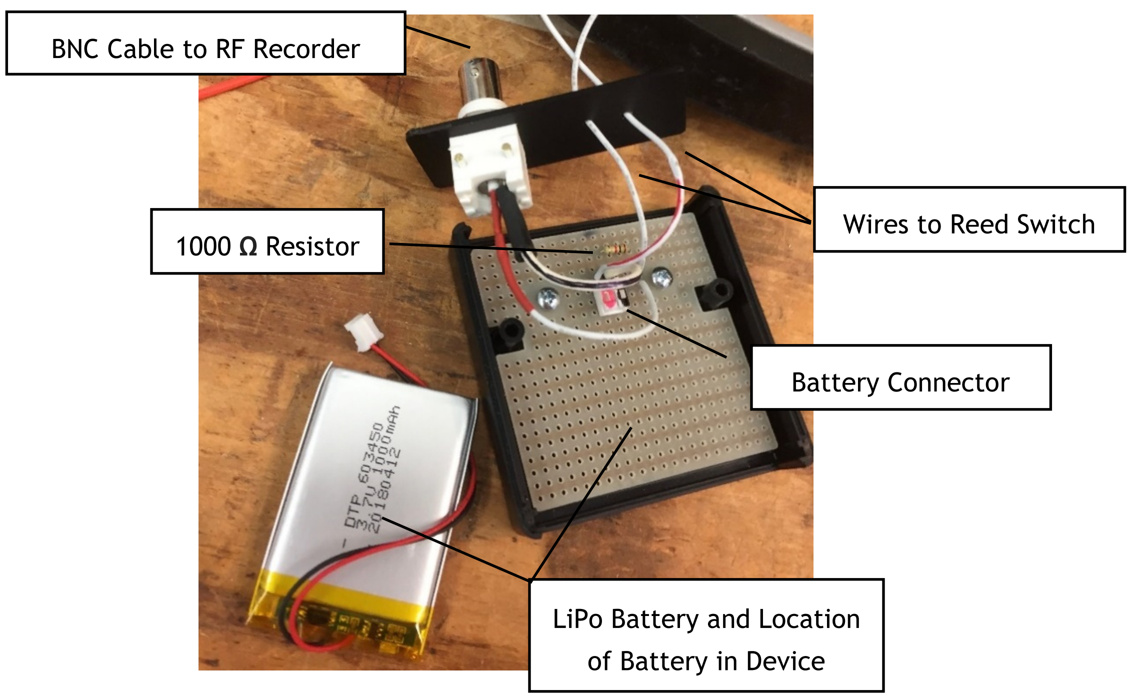

When the system is deployed in an area with good GPS reception (e.g., suburban, rural, or other open areas), the survey wheel can be replaced by GPS operating on the recording laptop. In this case, we use a terminal program to log the NMEA (National Marine Electronics Association) data stream to a text file in the background while the RF recorder is set to record data continuously. The GPS records position every second. In postprocessing, the GPS position data is merged with the RF recording using timestamps (the code is found in Appendix C).

3 Measurement Methods

3.1 Survey area

Measuring representative RF-noise power levels and spatial variability is critical for making accurate generalizations about urban RF noise. Because of its proximity to CRREL, we chose Boston, a major urban center of over 650,000 people (according to the 2016 census data), as the study site. Its downtown features dense, high-rise buildings that are used primarily as office buildings with some hotels and residential buildings as well. Boston's North End neighborhood is adjacent to downtown and features 4–5 story brick buildings, mostly residential and small business, lining narrow streets. The neighborhood is one of the oldest in Boston.

We chose two routes (shown in Figure 4 and Figure 5) to cover most of the major areas of the downtown and the North End. The routes are both just over 2 km long and can be walked within an hour, allowing for multiple laps at the each frequency so as to capture temporal variability.

Figure 4. Map of the survey area and route through downtown Boston, Massachusetts. The route is 2.14 km long. (Background map: © OpenStreetMap contributors.)

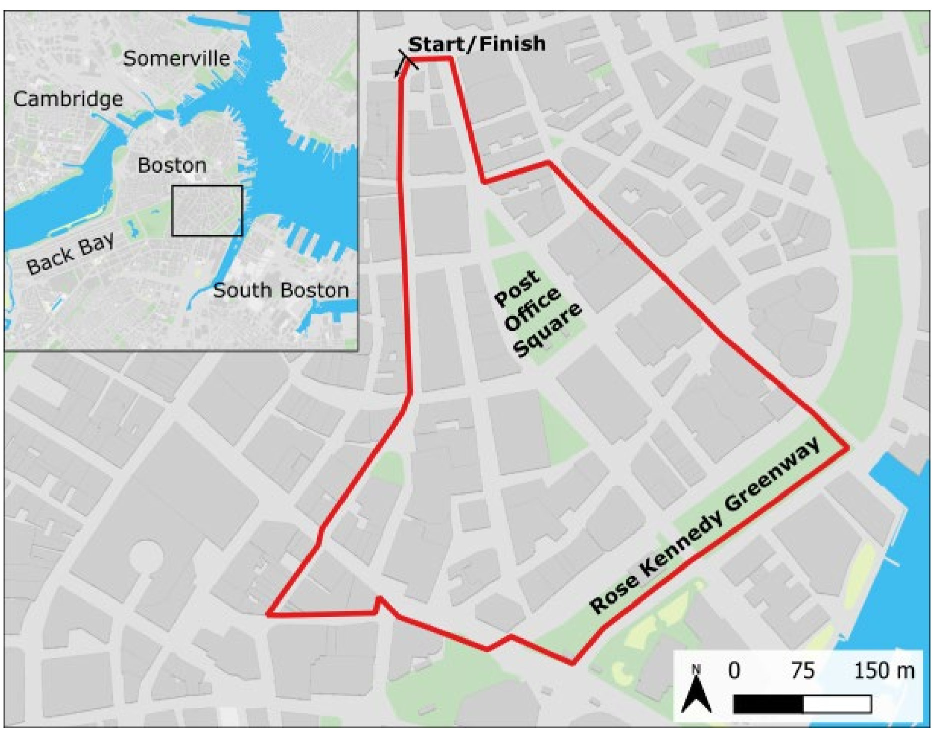

Figure 5. Map of the survey area and route through the North End of Boston, Massachusetts. The route is 2.32 km long. (Background map: © OpenStreetMap contributors.)

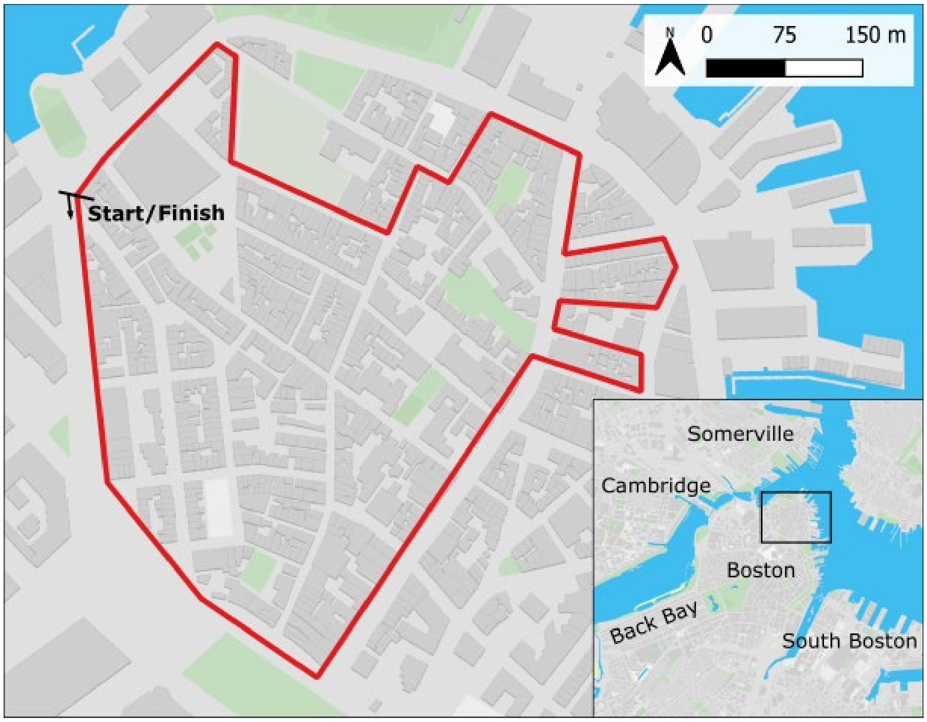

3.2 Spectrum survey

To select frequencies absent of intentional emitters, we conducted a spectrum survey during preliminary fieldwork in the summer of 2018. The RF recorder was put in spectrum analyzer mode and set to a lower sensitivity setting to prevent overloading the system when we encountered intentional emitters. The bandpass filters were tuned slowly across the spectrum from 63 MHz to 1000 MHz, changing filters as needed. As we moved across the spectrum, we identified frequencies that had no intentional emitters in a 1 MHz bandwidth or strong emitters immediately spectrally adjacent. With these frequencies, we conducted preliminary measurements along the downtown route to ensure there were no intermittent intentional emitters. After this, we identified three frequencies, 142, 246.5, and 972 MHz, as appropriate for noise measurements in this area. These frequencies have no strong emitters immediately adjacent and have no weak emitters within a 1 MHz bandwidth. These frequencies are also federally exclusive portions of the spectrum, which may help to explain their suitability for our noise measurements.

4 Results

Our results confirm that there is significant variation in noise power on the block scale in urban environments. We observed variations in median noise power ranging from 15 dB to 30 dB at each frequency in both neighborhoods. We also observed block-scale changes in peak power, the upper tail of our noise-power distribution. By repeating two laps at each frequency, 142, 246.5, and 972 MHz, we show that noise is generally consistent in both spatial extent and power during the day. At 142 MHz, we conducted an additional survey several weeks beforehand in downtown. The surveys, even separated by several weeks, have similar noise-power levels and spatial characteristics.

4.1 Median external noise power

Median external noise power, denoted Fam, has become the preferred statistic for describing noise-power levels (Achatz et al. 1998; Achatz and Dalke 2001; Dalke et al. 1997; Wepman and Sanders 2011; Wagstaff and Merricks 2005) because, unlike the mean, it will not be impacted by the presence of infrequent but powerful impulsive noises. We define median external noise power as the median power measured each meter.

Figures 6–8 map median external noise power. High median noise powers tend to form clusters. At 142 MHz, these high-powered clusters are hundreds of meters long. As frequency increases, the clusters appear to decrease in size. Clusters at 972 MHz are several meters long. The high-powered noise clusters also appear to be spatially correlated between different frequencies; areas with higher noise powers at one frequency will likely be elevated at other frequencies. This correlation is especially evident between 142 MHz and 246.5 MHz.

Figures 9–11 show the distributions of median external noise powers and associated statistics. At the frequencies we measured, median noise power decreases with frequency and, overall, is lower in the North End than in downtown. Data collected in the North End at 972 MHz is also influenced by the minimum system sensitivity.

Figure 6. Median external noise power in Boston's downtown (*top*) on 24 October and North End (*bottom*) on 10 October 2018 at 142 MHz. The second lap is shifted to be displayed alongside the first lap; the route walked was the same as the first lap. Areas labeled by A, B, and C are referenced in Fig. 17. Values below −97.8 dBm are too close to the system noise floor to be reliable. (Background map: © OpenStreetMap contributors.)

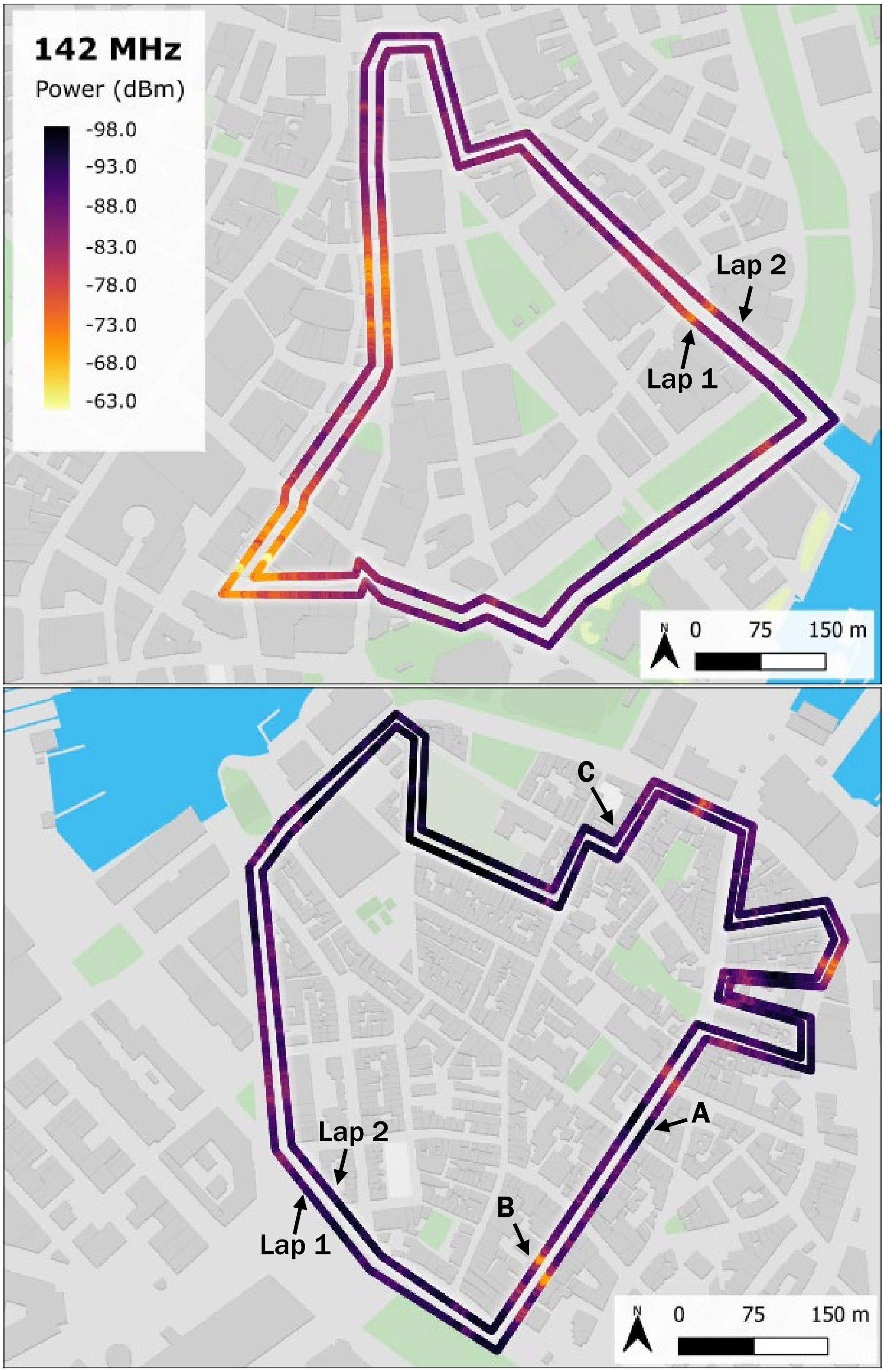

Figure 7. Median external noise power in Boston's downtown (*top*) on 9 October and North End (*bottom*) on 10 October 2018 at 246.5 MHz. The second lap is shifted to be displayed alongside the first lap; the route walked was the same as first lap. (Background map: © OpenStreetMap contributors.)

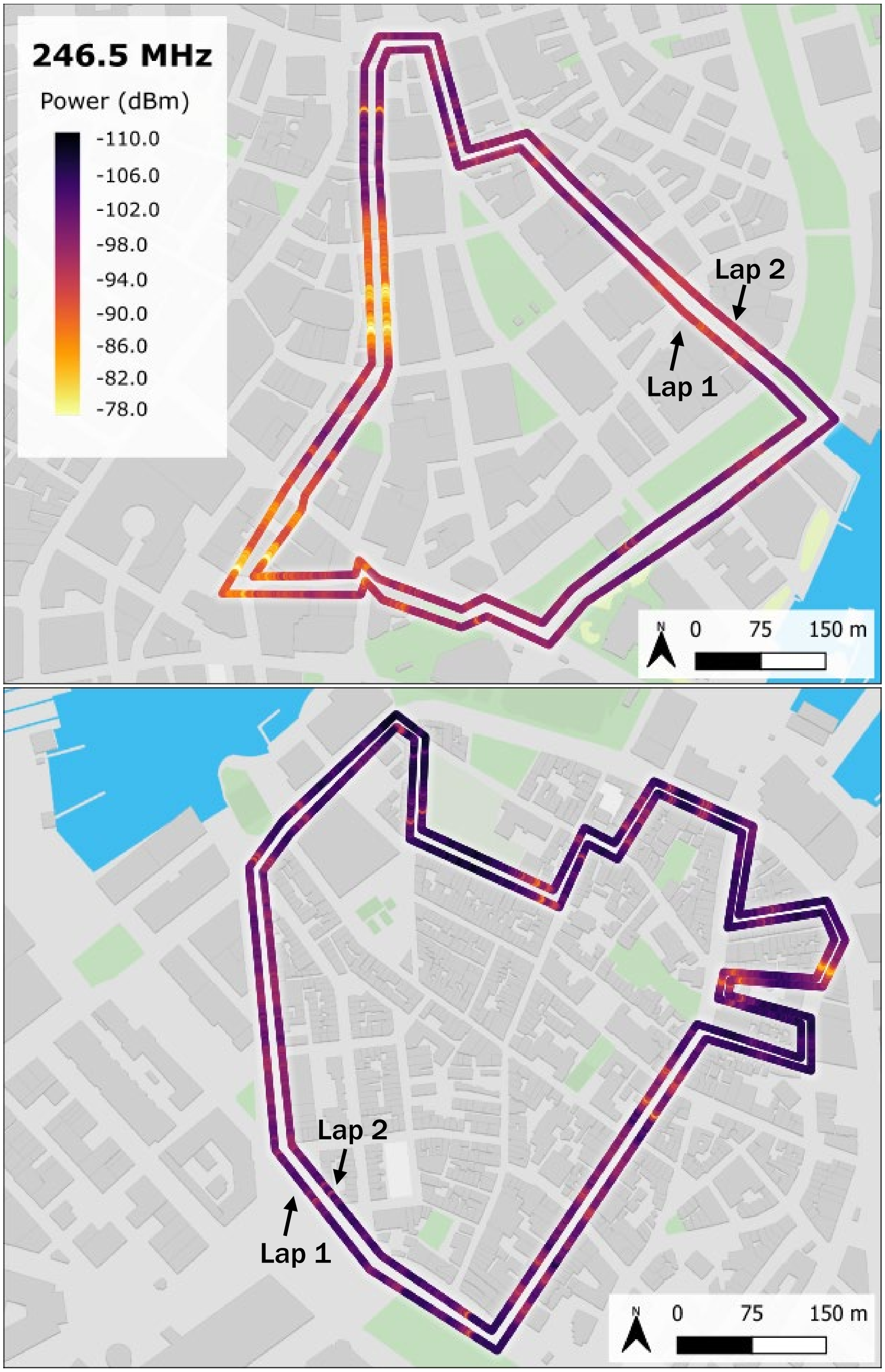

Figure 8. Median external noise power in Boston's downtown (*top*) on 9 October and North End (*bottom*) on 10 October 2018 at 972 MHz. The second lap is shifted to be displayed alongside the first lap; the route walked was the same as first lap. Values below −110.7 dBm are too close to the system noise floor to be reliable. (Background map: © OpenStreetMap contributors.)

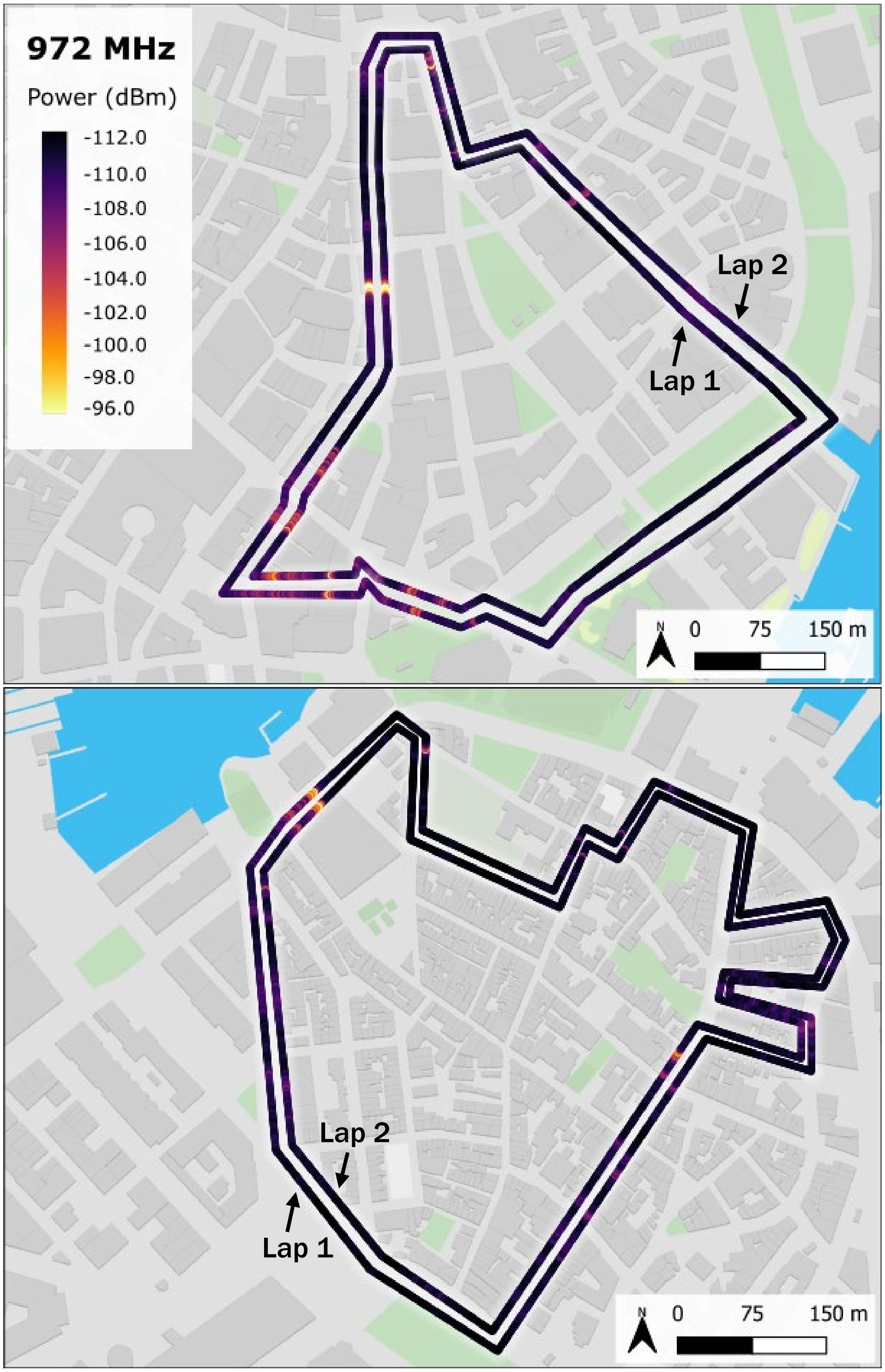

Figure 9. Histograms of median external noise power at 142 MHz for samples collected every meter throughout the North End (*bottom*) and downtown Boston (*top*) on 10 and 24 October, respectively. The *dashed line* is the minimum system sensitivity, 0.75 dB above the system noise.

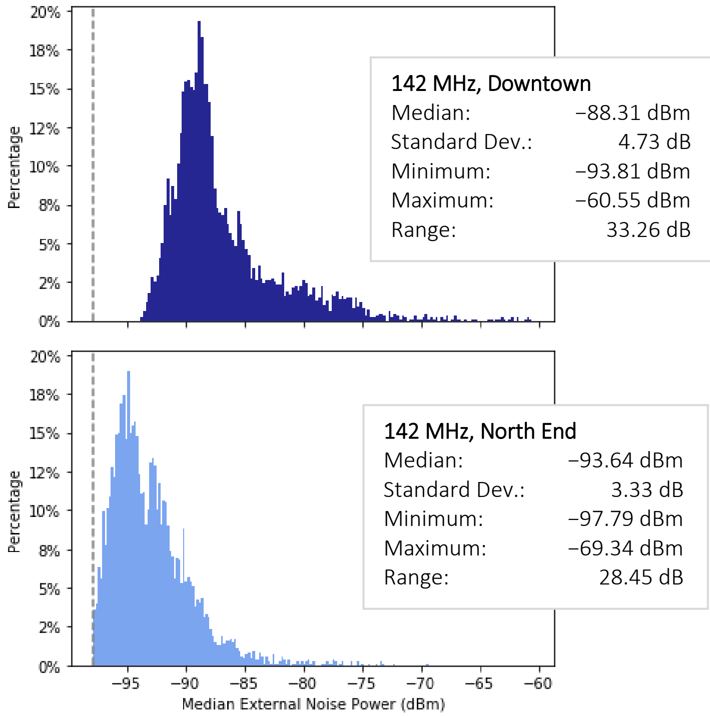

Figure 10. Histograms of median external noise power at 246.5 MHz for samples collected every meter throughout downtown Boston (*top*) and the North End (*bottom*) on 9 and 10 October, respectively. The *dashed line* is the minimum system sensitivity, 0.75 dB above the system noise.

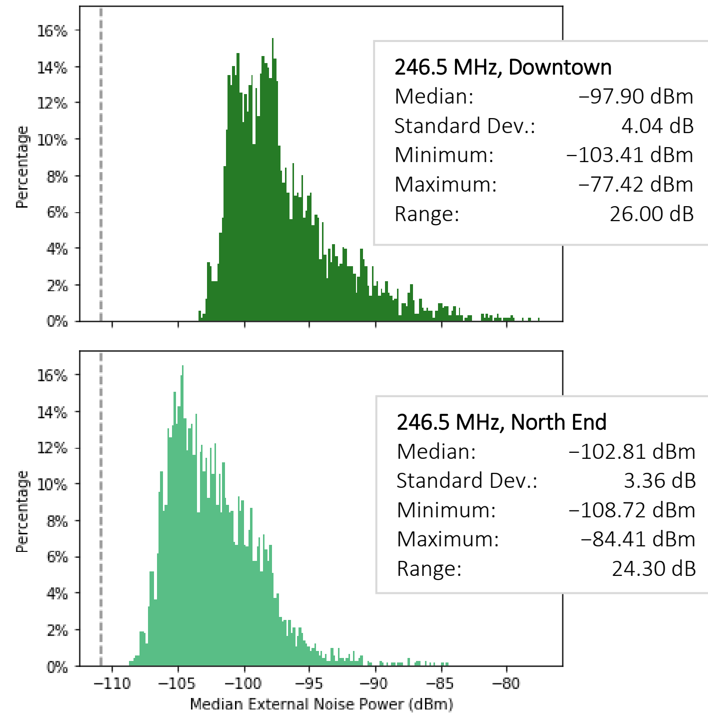

Figure 11. Histograms of median external noise power at 972 MHz for samples collected every meter throughout downtown Boston (*top*) and the North End (*bottom*) on 9 and 10 October, respectively. The *dashed line* is the minimum system sensitivity, 0.75 dB above the system noise. A significant portion of the data is at or near the system noise for both neighborhoods; therefore, we do not report overall statistics for this frequency.

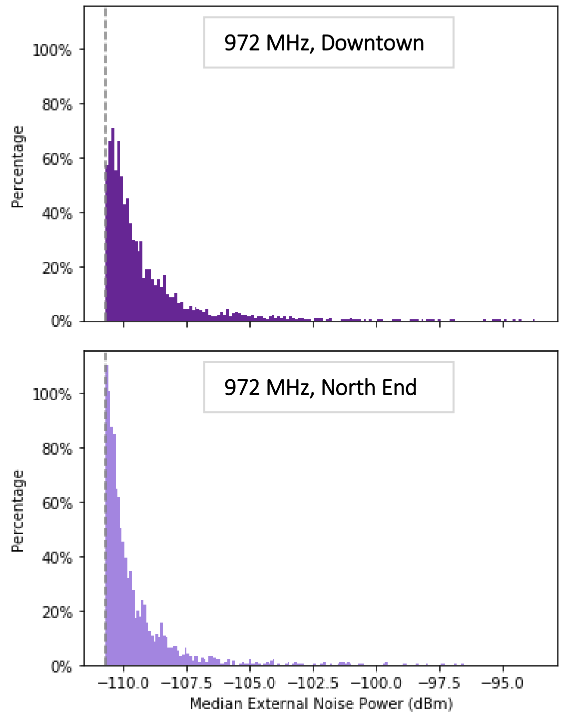

4.2 Peak power

Another way to statistically summarize extreme events in noise data is peak power. As in Achatz et al. (1998), Achatz and Dalke (2001), and Wepman and Sanders (2011), we define peak noise power as the noise-power level exceeded 0.01% of the time. Figures 12–14 map peak powers in the downtown and North End. Similar to median power, there is significant variability throughout each neighborhood, and higher peak powers form clusters.

Figure 12. Peak noise power at 142 MHz in downtown Boston (*top*) on 24 October and the North End (*bottom*) on 10 October. Letters are referenced in Fig. 17. (Background map: © OpenStreetMap contributors.)

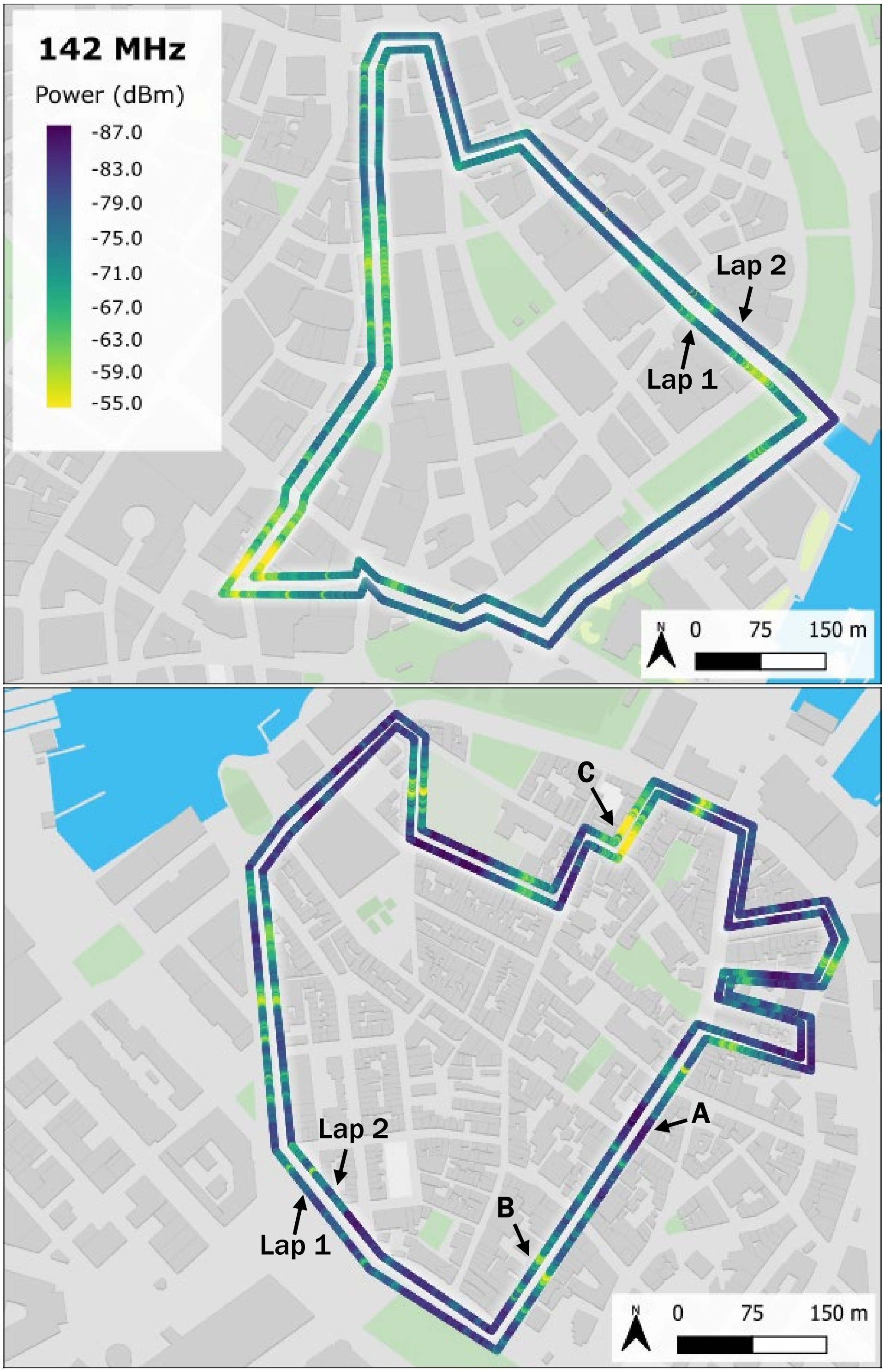

Figure 13. Peak noise power at 246.5 MHz in downtown Boston (*top*) on 9 October and the North End (*bottom*) on 10 October. (Background map: © OpenStreetMap contributors.)

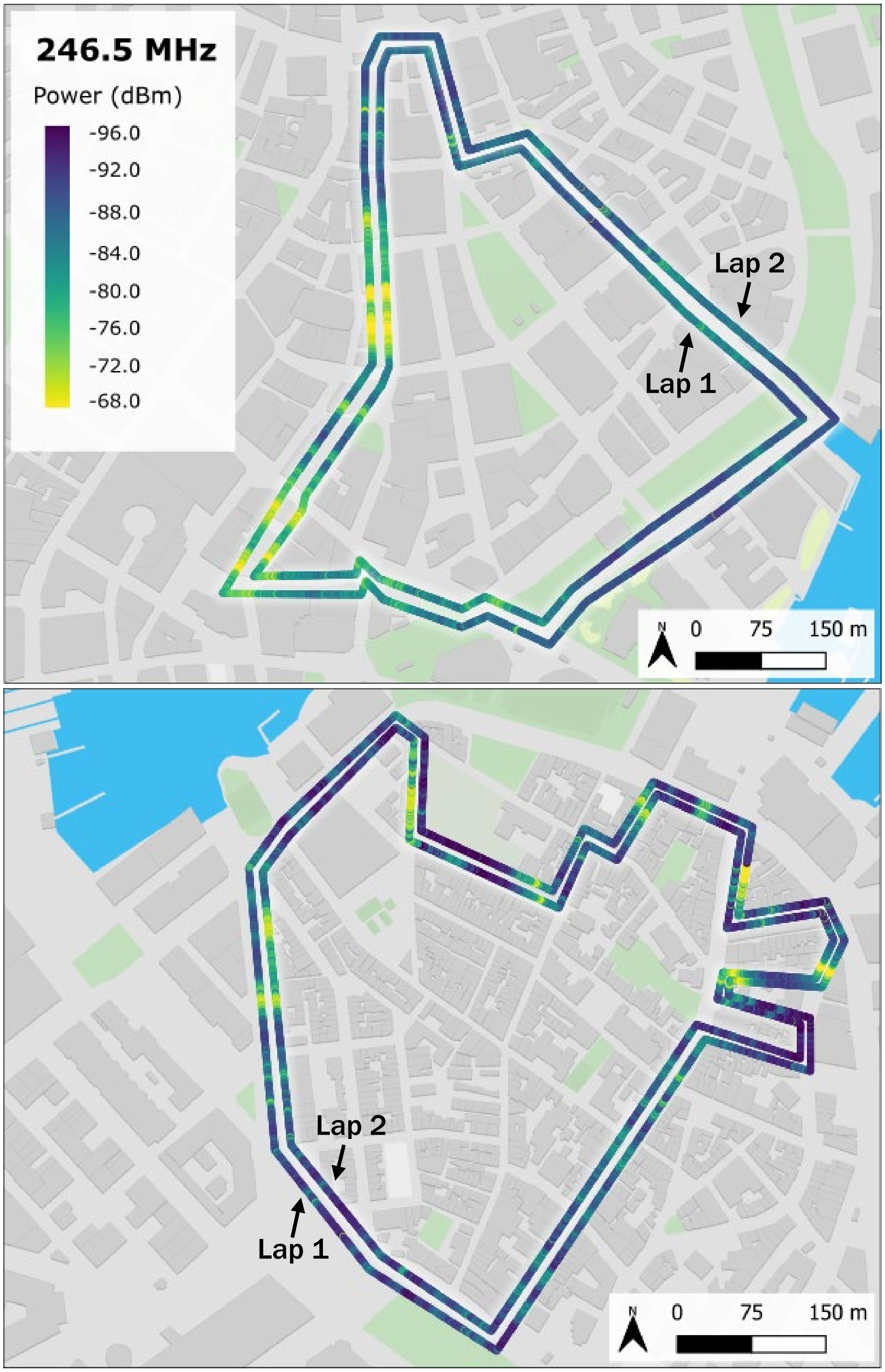

Figure 14. Peak noise power at 972 MHz in downtown Boston (*top*) on 9 October and the North End (*bottom*) on 10 October. (Background map: © OpenStreetMap contributors.)

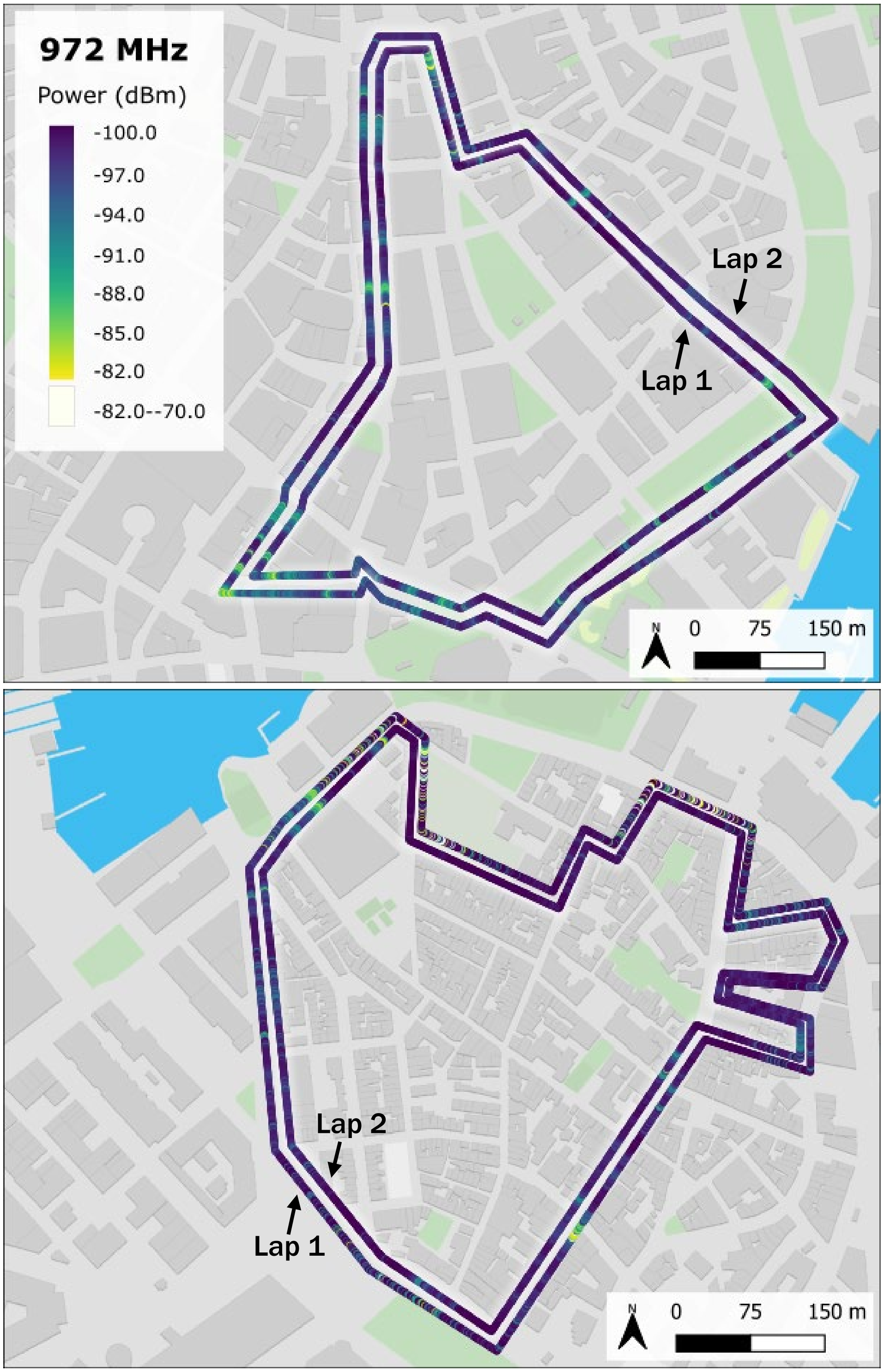

4.3 Temporal noise-power variability

Repeating the route at each frequency (142 MHz, 246.5 MHz, and 972 MHz) and conducting surveys at 142 MHz several weeks apart allows us to compare changes in median noise-power levels over time. All surveys were conducted during normal business hours on 9, 10, and 24 October; and there was about an hour between the start of each survey. Table 4 shows the date and time each survey started.

Table 4. Date and time of noise surveys. Times reported are start times; the laps take about an hour.

Frequency (MHz)	Downtown Lap 1	Downtown Lap 2	Downtown Lap 3	North End Lap 1	North End Lap 2
142	24 Oct. 9:55 a.m.	24 Oct. 10:55 a.m.	9 Oct. 11:05 a.m.	10 Oct. 7:44 a.m.	10 Oct. 8:44 a.m.
246.5	9 Oct. 1:53 p.m.	9 Oct. 3:41 p.m.		10 Oct. 9:28 a.m.	10 Oct. 10:15 a.m.
972	9 Oct. 5:00 p.m.	9 Oct. 5:41 p.m.		10 Oct. 11:58 a.m.	10 Oct. 12:42 p.m.

The median noise-power levels did not change significantly between surveys as shown in Figure 15. Clusters of high noise powers are present in both laps and often have corresponding peaks at other frequencies. At 142 MHz, we conducted surveys on 9 and 24 October 2018, allowing us to compare median noise-power levels across weeks (Figure 16). The correlation is not as strong as the laps conducted on the same day, but the trend is consistent; median noise powers are a function of location even in surveys conducted weeks apart.

Figure 15. Median noise power varying with distance along the route in Boston's downtown (*top*) and North End (*bottom*). Power levels are consistent between laps completed an hour apart.

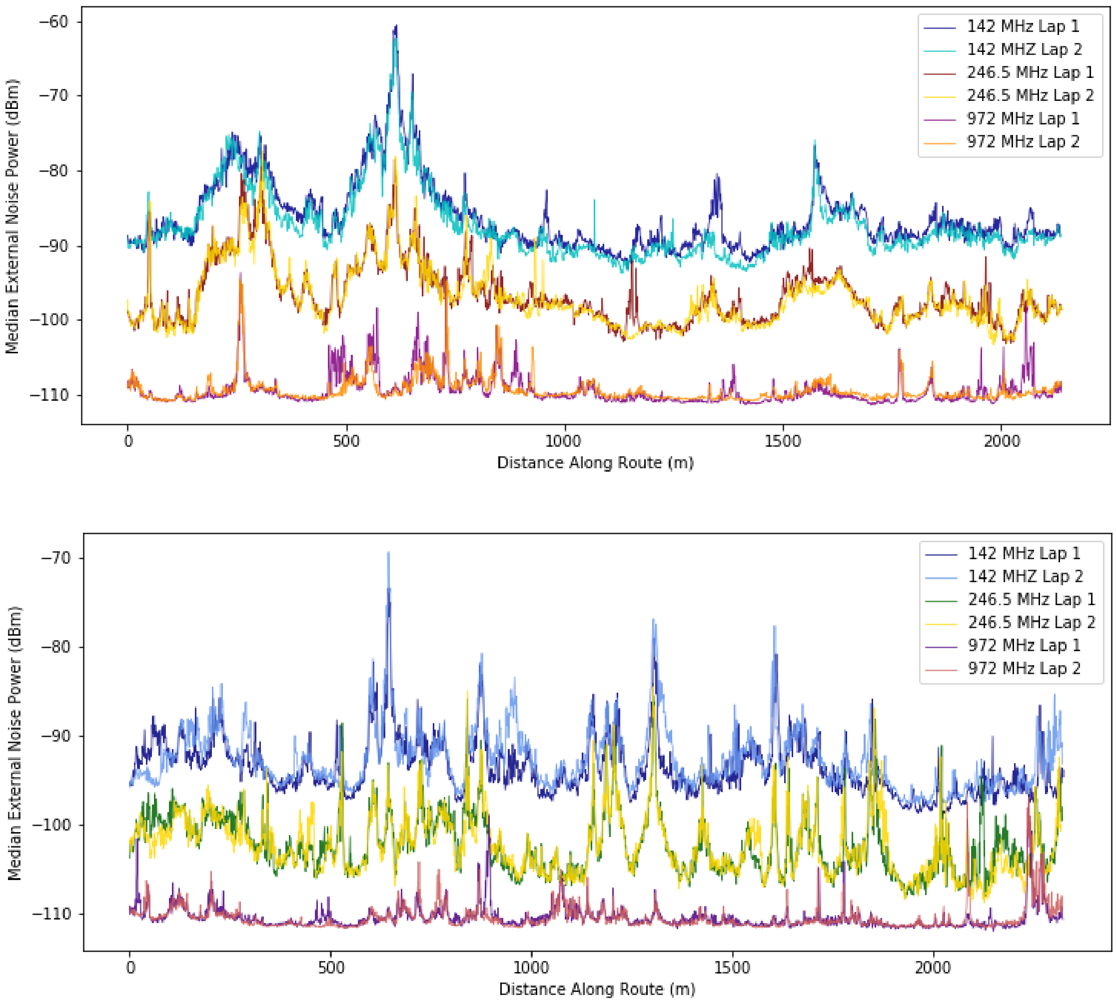

Figure 16. Median noise-power levels in downtown Boston from surveys taken 2 weeks apart at 142 MHz. Power levels are generally consistent between weeks.

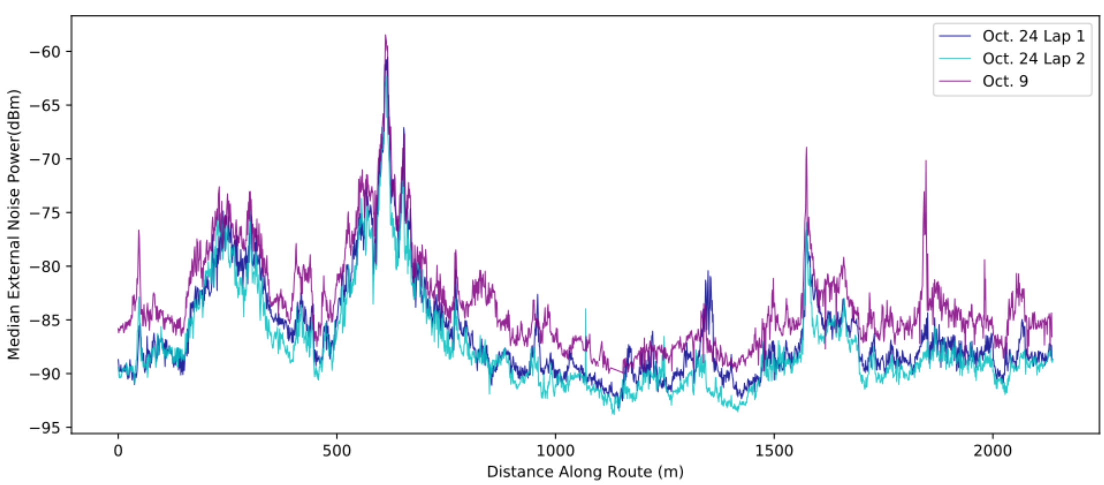

5 Discussion

Our results show, for the first time, significant and repeatable spatial variation in noise power throughout the urban environment. We found median noise power varied more than 15 dB within each neighborhood at all frequencies measured. This variability is within a few decibels of or larger than variability between business and residential locations reported in previous studies (Achatz and Dalke 2001; Wagstaff and Merricks 2005; Wepman and Sanders 2011), suggesting that stationary measurements are unlikely to capture representative neighborhood noise levels. Accurate noise-level characterization requires multiple, spatially distributed measurements, covering distances of several thousand wavelengths with high enough density to resolve noise clusters on the order of tens of wavelengths long.

5.1 Temporal variability in noise power

Our surveys indicate that the spatial distribution of noise powers is consistent during business hours. Surveys conducted an hour apart and even weeks apart show similar clustering of high noise power. This consistency suggests that patterns in noise power are not from temporally discrete events such as a noisy passing vehicle but enduring features of the urban noise field. Wepman and Sanders (2011) show noise powers decrease outside of business hours in a business district of Denver. To make better generalizations about RF-noise levels and their spatial patterns, measurements would need to be conducted during the evenings, nights, and weekends.

5.2 Spatial variability in noise power

We observed clusters of high median noise powers in both neighborhoods and at all frequencies. These clusters are 300–500 m apart, but a more extensive survey is necessary to accurately report the average distances between clusters. This distance could be a useful figure for describing the urban noise field. The high-powered clusters are related to the surrounding environment although we do not know their sources. In open areas, such as the Rose Kennedy Greenway, a long park near the waterfront in downtown, we consistently find our lowest median noise powers at each frequency. In the narrow urban canyons, surrounded by tall office buildings, we find our most powerful clusters. The clusters are between 30 and 50 wavelengths long. Thus, higher frequencies have smaller clusters than lower frequencies. In the North End, the high-powered clusters are smaller in length (about 10 wavelengths) but occur at similar intercluster spacing. Overall, the fine-scale spatial variability of noise suggests that the urban noise field is composed of many sources located at irregular intervals throughout the urban environment.

Peak power also varies significantly throughout both the downtown and North End *but does not always vary proportionately to median power*. We find the relationship between peak power and median power can be grouped in three categories: low peak power / low median power, high peak power / high median power, and high peak power / low median power. These three categories can easily be seen on a plot of peak power and median power (example shown in Figure 17). Red crosses in Figure 17 represent data collected from a calibrated thermal noise source. The noise source generates Gaussian noise; and, as the median increases, the peak power increases proportionately (in milliwatts). Regions A and B (low/low and high/high) both fall on the thermal noise line. Region C has a strong impulsive component relative to its median power, resulting in high peak powers. Examples of regions A, B, and C are found on the maps for 142 MHz in the North End in Figures 6 and 12.

Figure 17. Median power and peak power (0.01%) at 142 MHz in Boston's North End shows the presence of impulsive noise. Points in regions A and B are dominated by Gaussian noise. Points in region C have strong impulsive components. The cluster of points at −54 dBm is at the maximum system sensitivity.

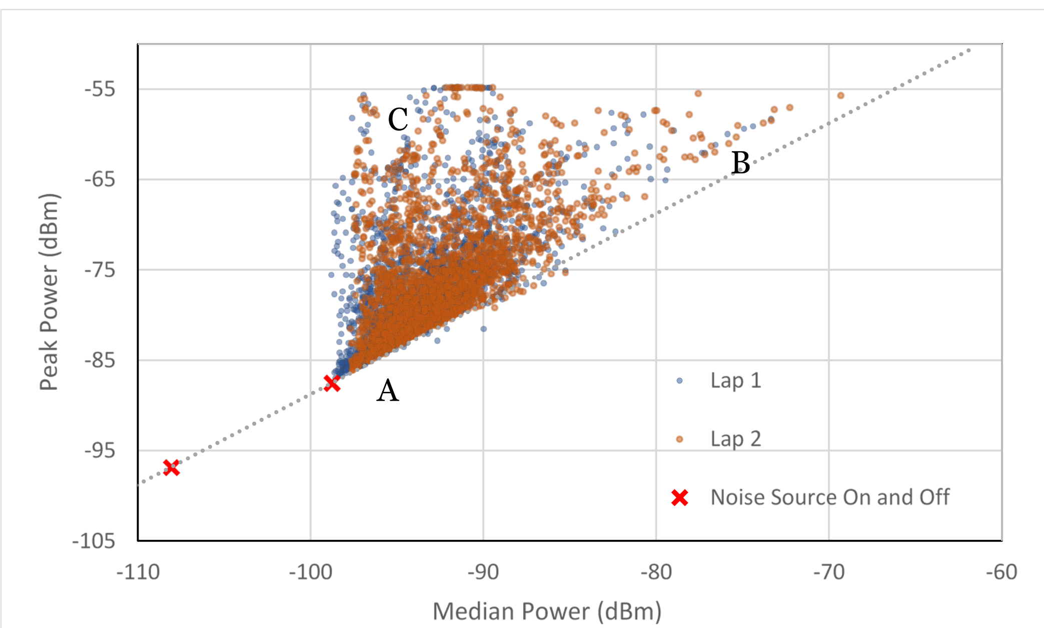

5.3 Comparison to the ITU model and previous studies

The ITU (2016) recommendation on radio noise briefly discusses variability of noise power between locations. They report upper and lower decile deviations of 8.4 dB in urban environments at frequencies between 0.3 and 250 MHz. While it is unclear what type or scale of location variability the report is referencing or how the report defines upper and lower deciles deviation, we define them here as the 10th and 90th percentile of our median noise powers (F_{am}). We find the difference between the first decile and the median to be 2.82 and 3.10 dB (lower decile deviation) and 8.35 and 6.81 dB between the last decile and the median (upper decile deviation) for 142 MHz and 246.5 MHz, respectively, in downtown Boston. Contrary to the assumption of ITU-R P.372, the large difference between our lower and upper decile deviations shows that our observed variation in median noise power (F_{am}) is not Gaussian (Figures 9–11) as assumed by the ITU's symmetrical, Gaussian variation of 8.4 dB. ITU-R P.372 (2016) does not discuss expected noise variability above 250 MHz. While other studies (Wagstaff and Merricks 2005; Wepman and Sanders 2011; Achatz and Dalke 2001) address temporal variations in median noise power (F_{am}) and variation in noise power (F_a), spatial variation at the subcity scale is unreported except for ITU's brief mention.

Our results were consistently 5 to 10 dB higher than the ITU model, indicating that the urban noise field may have evolved since the measurements of Spaulding and Disney (1974) and revisions of the ITU model (2016). Wepman and Sanders (2011) conducted stationary, 1 MHz bandwidth measurements in a business neighborhood of Denver, Colorado, during the summer of 2009. Achatz and Dalke (2001) conducted a similar study in Denver at 137.5 MHz. Although recording duration, frequencies, and methodologies vary, in Table 5, we compare our results to those from other studies and the ITU model.

Table 5. Comparison of median external noise values.

Frequency (MHz)	Downtown Boston (dBm)	North End Boston (dBm)	Wepman and Sanders (2011) Business (dBm)	Achatz and Dalke (2001) Business (dBm)	ITU Model Business (dBm)	ITU Model Residential (dBm)
112.5			−85.9		−93.99	−98.29
137.5				−96.4	−96.41	−100.70
142	−88.31	−93.72			−96.79	−101.09
221.5			−99.1		−102.14	−106.44
246.5	−97.90	−102.81			−103.43	−107.73
972	*	*			−111.2	Below thermal noise floor

* F_{am} values are at system noise floor.

6 Conclusion

The mobile noise measurement system presented in this paper can measure frequencies between 63 MHz and 1 GHz with a 1 MHz bandwidth at spatial resolutions down to 1 m. We deployed the system in Boston, Massachusetts, in both the downtown and the historic North End neighborhoods. Measurements showed significant spatial variation in median noise powers within each neighborhood of at least 15 dB and as high as 33 dB across three measured frequencies, 142, 246.5, and 972 MHz. There was also a significant difference in the adjacent neighborhoods' overall median noise powers. The results show that spatial variability is a critical factor in determining representative noise levels for urban environments, implying that future noise studies should include measurements throughout the neighborhood of interest with a density high enough to resolve clusters of noise powers on the scale of a few wavelengths. Stationary measurements, as are commonly reported in the literature, are unlikely to capture representative levels.

More surveys of downtown Boston and the North End are needed to find representative noise levels. The data shown here was collected during business hours at only three frequencies. The routes used for data collection are transects through a complex urban noise field; denser surveys that cover each neighborhood at a resolution of several wavelengths are needed to accurately capture the variability. Planned future surveys will increase the number of frequencies measured to better represent frequency-dependent spatial noise-power variability. Additionally, we plan to conduct measurements at different times of the day.

Man-made RF noise is a critical parameter for predicting the performance of communication systems and electromagnetic sensors in urban environments. The significant spatial variability we found in Boston provides important information for future studies hoping to characterize urban RF-noise levels. These results also indicate that more work is needed to develop our understanding of urban RF-noise variability.

References

Achatz, R. J., and R. A. Dalke. 2001. *Man-Made Noise Power Measurements at VHF and UHF Frequencies*. NTIA Report 02-390. Boulder, CO: U.S. Department of Commerce, National Telecommunications and Information Administration. https://www.its.bldrdoc.gov/publications/download/TR-02-390.pdf.

Achatz, R., Y. Lo, P. Papazian, R. Dalke, and G. Hufford. 1998. *Man-Made Noise in the 136 to 138-MHz VHF Meteorological Satellite Band*. NTIA Report 98-355. Boulder, CO: U.S. Department of Commerce, National Telecommunications and Information Administration. https://www.its.bldrdoc.gov/publications/download/TR-98-355.pdf.

Dalke, R., R. Achatz, Y. Lo, P. Papazian, and G. Hufford. 1997. "Measurement and Analysis of Man-Made Noise in VHF and UHF Bands." In *Proceedings of the 1997 Wireless Communications Conference*, 11-13 August, Boulder, CO, 229–233.IEEE. https://doi.org/10.1109/WCC.1997.622284.

Fairview Microwave. 2018. "*Calibrated Noise Source Module With a Noise Output ENR of 15 dB, and a Voltage of +28 VDC, Operating From 10 MHz to 6 GHz With SMA*." User Manual. Lewisville, TX: Fairview Microwave. https://www.fairviewmicrowave.com/images/productPDF/FMNG1021.pdf

Hagn, G. H., and D. B. Sailors. 1979. "Empirical Models for Probability Distributions of Short-Term Mean Environmental Man-Made Radio Noise Levels." In *Proceedings of the 3rd Symposium and Technical Exhibition on Electromagnetic Compatability*, 355–360.

Hess, G. C. 1998. *Handbook of Land-Mobile Radio System Coverage*. Norwood, MA: Artech House.

ITU (International Telecommunication Union). 2016. *Radio Noise*. Recommendation ITU-R P.372-13. Geneva, Internation Telecommunications Union, Radiocommunications Sector. https://www.itu.int/dms_pubrec/itu-r/rec/p/R-REC-P.372-13-201609-I!!PDF-E.pdf.

Keysight Technologies. 2019. *Noise Figure Measurement Accuracy: The Y-Factor Method*. Application Note. Colorado Springs, CO: Keysight Technologies. http://literature.cdn.keysight.com/litweb/pdf/5952-3706E.pdf.

Leferink, F., F. Silva, J. Catrysse, S. Batterman, V. Beauvois, and A. Roc'h. 2010. "Man-Made Noise in Our Living Environments." *Radio Science Bulletin* 334: 49–57.

Norton, K. A. 1953. "Transmission Loss in Radio Propagation." In *Proceedings of the IRE*, 146–152. https://ieeexplore.ieee.org/stamp/stamp.jsp?tp=&arnumber=4051172&tag=1.

Oliphant, T. E. 2006. *A Guide to NumPy*. Trelgol Publishing.

Seybold, J. S. 2005. *Introduction to RF Propagation*. Hoboken, NJ: John Wiley & Sons, Inc. https://onlinelibrary.wiley.com/doi/book/10.1002/0471743690.

Spaulding, A. D., and R. T. Disney. 1974. *Man-Made Radio Noise, Part 1: Estimates for Business, Residential, and Rural Areas*. OT Report 74-38. Boulder, CO: U.S. Department of Commerce, Office of Telecommunications. https://www.its.bldrdoc.gov/publications/download/OT-74-38.pdf.

Wagstaff, A., and N. Merricks. 2005. "Man-Made Noise Measurement Programme." *IEE Proceedings - Communications* 152 (3): 371–377. https://doi.org/10.1049/ip-com:20045025.

Wepman, J. A., and G. A. Sanders. 2011. *Wideband Man-Made Radio Noise Measurements in the VHF and Low UHF Bands*. NTIA Technical Report TR-11-478. Boulder, CO: U.S. Department of Commerce, National Telecommunications and Information Administration. http://www.its.bldrdoc.gov/publications/2553.aspx.

Appendix A: Noise Figures and Y-Factor Method

We used the Y-factor method to find the internal noise figures and gains for each component and the total system. The Y-factor method uses a calibrated noise diode and different system configurations to isolate each component. We began with the noise source connected directly to the RF recorder and took measurements with the source turned on for 1 minute and then off for 1 minute. We repeated the procedure with the preamplifier and tunable bandpass filters inserted, one at a time, between the noise source and the RF recorder. Table A-1 provides the average powers for each measurement.

Table A-1. Y-factor method measurements. The reported powers are the average over a 1-minute recording.

Frequency (MHz)	RF Recorder with Noise Source				Preamplifier and RF Recorder with Noise Source			
	On		Off		On		Off	
	dBm	mW	dBm	mW	dBm	mW	dBm	mW
142	−93.6	4.35E−10	−95.8	2.65E−10	−66.68	2.15E−07	−79.36	1.16E−08
246.5	−93.8	4.21E−10	−95.9	2.58E−10	−67.07	1.96E−07	−79.47	1.13E−08
972	−93.6	4.41E−10	−95.3	2.93E−10	−68.19	1.52E−07	−79.87	1.03E−08

Frequency (MHz)	Filters and RF Recorder with Noise Source				Total System with Noise Source			
	On		Off		On		Off	
	dBm	mW	dBm	mW	dBm	mW	dBm	mW
	125–250 MHz Filter				125–250 MHz Filter			
142	−94.7	3.38E−10	−95.6	2.74E−10	−70.1	9.77E−08	−79.4	1.14E−08
246.5	−94.6	3.50E−10	−95.7	2.68E−10	−69.5	1.12E−07	−79.5	1.11E−08
	500–1000 MHz Filter				500–1000 MHz Filter			
972	−93.9	4.03E−10	−95.2	3.00E−10	−69.0	1.27E−07	−79.8	1.04E−08

The Y-factor method leverages the fact that noise power can be described using an effective temperature. Instead of using power to calculate the noise factor (which is typically described as a ratio between the input SNR and the output SNR), we can use an equivalent temperature and get the same ratio (equivalent temperature over room temperature).

The Y-factor is a ratio of the noise power with the noise diode turned on (N_{on}) and off (N_{off}):

$$y = \frac{N_{on}}{N_{off}} = \frac{t_{on}}{t_0}.$$

To find the noise figure of our receiver, we begin with the excess-noise ratio (ENR) of our calibrated noise source, which is defined as

$$ENR = \frac{(t_{on} - t_0)}{t_0},$$

where

t_{on} = the equivalent temperature of the noise source and
t_o = the noise source temperature when powered off (room temperature).

ENR values are reported in the manual of a calibrated noise source. We use a Fairview Microwave Calibrated Noise Source (product number FMNG1021) (Fairview Microwave 2018) with effective noise ratio (ENR) values in Table A-2.

Table A-2. Excess-noise ratio (ENR) of the Fairview Microwave Calibrated Noise Source.

Frequency (MHz)	ENR (K)
142 MHz	12933.28
246.5 MHz	12692.33
972 MHz	11141.48

By setting t_o = 295 K, we find t_{on} for each frequency.

Using our calibration measurement, we can find the noise factor of the receiver and our total system (Table A-3).

Table A-3. RF recorder and total system noise figure calculations.

Description	Equation	Frequency	RF Recorder	Total System
Y-Factor	$y_2 = \frac{N_{on}}{N_{off}}$	142	1.64 dB	8.53 dB
		246.5	1.63 dB	10.12 dB
		972	1.50 dB	12.22 dB
Effective Temperature	$t_2 = \frac{(t_{on} - y_2 t_0)}{(y_2 - 1)}$	142	19550.64 K	1383.00 K
		246.5	19404.92 K	1064.82 K
		972	21411.19 K	671.72 K
Noise Figure	$f = 1 + \frac{t_2}{t_0}$	142	18.28 dB	7.55 dB
		246.5	18.25 dB	6.64 dB
		972	18.67 dB	5.15 dB

With the noise figure of the RF recorder, we can determine the gain and noise figure of our preamplifier and filters, as shown in Table A-4.

Table A-4. Component noise figure calculations.

			Configuration		
Description	Equation	Frequency (MHz)	RF Recorder and Preamplifier	RF Recorder and Filter 125–250	RF Recorder and Filter 500–1000
Y-factor	$y_{12} = \frac{N_{on}}{N_{off}}$	142	18.54 dB	1.24 dB	
		246.5	17.38 dB	1.31 dB	
		972	14.72 dB		1.34 dB
Combined Effective Temperature	$t_{12} = \frac{(t_{on} - y_{12} t_0)}{(y_{12} - 1)}$	142	425.57 K	53268.18 K	
		246.5	461.79 K	40195.89 K	
		972	495.22 K		31348.49 K
Component Gain	$g_1 = \frac{(N_{12}^{on} - N_{12}^{off})}{(N_2^{on} - N_2^{off})}$	142	30.80 dB	-4.18 dB	
		246.5	30.56 dB	-2.97 dB	
		972	29.84 dB		−1.54 dB
Component Effective Temperature	$t_1 = t_{12} - \frac{t_2}{g_1}$	142	409.31 K	2057.55 K	
		246.5	444.75 K	1754.15 K	
		972	472.99 K		845.62 K
Component Noise Figure	$f = 1 + \frac{t_{on}}{t_0}$	142	3.78 dB	9.02 dB	
		246.5	3.99 dB	8.42 dB	
		972	4.15 dB		5.8 dB

Appendix B: Geolocation with Survey Wheel Code

To use the 1 m measuring wheel for geolocations, we assume we will walk in predetermined straight lines connected by vertices while we are collecting data. This method relies on interpolating straight lines between known coordinates and would not work well if we walked curving paths through a park, for example.

The Python code with the NumPy library (Oliphant 2006) below outlines the process of matching files recorded by the RF recorder each meter with coordinates for each of those meters.

```
############################################
#Declarations
import numpy as np
import os

############################################
# Inputs

vertices = 'verts.txt'  #txt file with coordinates of each corner along
                          the route beginning at the same place the RF
                          recorder began collecting data. Each row has
                          latitude-longitude coordinates and number of
                          meters traveled to get to the corner.

files = os.listdir(path) #array of all RF recorder files collected along
                        vertices.

############################################
# Interpolation Function

# This function creates creating coordinates for each meter along the
route. The input is the coordinates and distance (meters) along the route
of each corner.
```

```
def interp_coords(corner_lat, corner_lon, corner_meters):
    meters, lats, lons = []

    for i in range(len(corner_meters)):
        #Find sections w/o coordinates (Lat = 0)
        meter_seg = np.arange(corner_meters[i], corner_meters[i+1])

        lat_seg = np.interp(meter_seg, (meter_seg[0], meter_seg[-1]),
                                       (corner_lat[i], corner_lat[i+1]) )

        lon_seg = np.interp(meter_seg, (meter_seg[0], meter_seg[-1]),
                                       (corner_lon[i], corner_lon[i+1]) )

        meters.extend(meter_seg)
        lats.extend(lat_seg)
        lons.extend(lon_seg)

    return meters, lats, lons

############################################
# Main Process

# create arrays from text file with route vertices
corner_lat, corner_lats, corner_meters = np.genfromtxt(vertices)

# Interpolate remaining coordinates along route
lats, lons = interp_coords(corner_lat, corner_lats, corner_meters)

############################################
# Now, the files, ordered by creation date, will line up with
corresponding latitude, longitude and meter along route at which it was
created. For example, the ith file was recorded at (lats[i], lons[i]) in
meter[i].
```

Appendix C: Geolocation Code for GPS

When the noise measurement system is configured to use the GPS, the RF recorder records continuously. The Python script presented below finds 1 second slices of the RF data collected at each GPS point.

```
# Variables
# GPStimes = GPS timestamps array in same timezone as RF Recorder
# lat = Latitudes array for each GPStimes
# lon = Longitudes array for each GPStimes
# rec_start_time = time that RF recording started
# sr = sample rate of RF recording in Hz
# sn = number of samples in RF recording
# power = array of powers in RF recording

import numpy as np

# Make Time Array for RF Recording in seconds
t = np.linspace(0, sn/sr, num = sn )

# Convert Time Array to Timestamps (seconds since epoch)
t = t + rec_start_time

# Next, we'll make GPS timestamp, latitude and longitude arrays
# where all the points were collected within RF recording's time
# range.
# We start by finding first and last second of RF Recording.
t_start = t[int(sr/2)]  #middle of 1st second of RF recording
t_stop  = t[-int(sr/2)] #middle of last second

# Next, we find the index of the nearest GPS timestamps to the
# beginning and end of the RF Recording
gps_start = np.searchsorted(GPStimes, t_start, side = "left")
gps_stop  = np.searchsorted(GPStimes, t_stop, side = "left")

# Then, we make our smaller GPS timestamp, latitude and longitude
# arrays that line up with the RF recording.
Gt = GPStimes [gps_start : gps_stop]
lat_sub = lat [gps_start : gps_stop]
lon_sub = lon [gps_start : gps_stop]
```

```
# Lastly, we find the powers and timestamps from the RF recording
# that were collected within a 0.5 seconds (1 second total) of
# each GPS point.

for time in Gt:
    #Find the closest RF Recording timestamp to the GPS
    # timestamp; returns index.
    t_center = np.searchsorted(t, time, side='left')

    # Find the index of the timestamp 0.5 seconds before the GPS
    # timestamp and 0.5 seconds after.
    t_start = int(t_center - sr/2)
    t_stop  = int(t_center + sr/2)

    # Finally, create arrays from the RF Recording timestamps and
    # powers that are within 0.5 seconds of the GPS point
    t_subset  = t [t_start : t_stop]
    power_subset = power[t_start : t_stop]

# With power_subset, we can find median external noise and other
statistics for the distribution for each GPS point.
```

REPORT DOCUMENTATION PAGE

Form Approved
OMB No. 0704-0188

1. REPORT DATE *(DD-MM-YYYY)* June 2019	**2. REPORT TYPE** Technical Report/Final	**3. DATES COVERED** *(From - To)*

4. TITLE AND SUBTITLE Measuring Very High Frequency and Ultrahigh Frequency Radio Noise in Urban Environments: A Mobile Measurement System for Radio-Frequency Noise	**5a. CONTRACT NUMBER** **5b. GRANT NUMBER** **5c. PROGRAM ELEMENT NUMBER**
6. AUTHOR(S) Caitlin E. Haedrich and Daniel J. Breton	**5d. PROJECT NUMBER** 61110252C00 **5e. TASK NUMBER** **5f. WORK UNIT NUMBER**
7. PERFORMING ORGANIZATION NAME(S) AND ADDRESS(ES) U.S. Army Engineer Research and Development Center (ERDC) Cold Regions Research and Engineering Laboratory (CRREL) 72 Lyme Road Hanover, NH 03755-1290	**8. PERFORMING ORGANIZATION REPORT NUMBER** ERDC/CRREL TR-19-8
9. SPONSORING / MONITORING AGENCY NAME(S) AND ADDRESS(ES) Headquarters, U.S. Army Corps of Engineers Washington, DC 20314-1000	**10. SPONSOR/MONITOR'S ACRONYM(S)** USACE **11. SPONSOR/MONITOR'S REPORT NUMBER(S)**

12. DISTRIBUTION / AVAILABILITY STATEMENT

Approved for public release; distribution is unlimited.

13. SUPPLEMENTARY NOTES

ERDC 6.1 Basic Research

14. ABSTRACT

Radio-frequency (RF) background noise is an important parameter in designing and predicting performance of RF communication and sensor systems. Modern man-made RF noise consists of unintentional emissions from sources such as electronic devices, power transmission lines, and internal combustion engine ignitions. Governments and academia have previously measured RF noise at fixed, representative locations within the urban environment. Considering the heterogeneous mix of office buildings, retail and residential buildings, transportation hubs, and parks that compromise modern cities, we hypothesize that RF-noise power varies significantly throughout the urban environment.

To characterize this variability, we present a mobile, tunable RF-noise measurement system designed to record frequencies from 63 MHz to 1 GHz in a 1 MHz to 10 MHz bandwidth. This report describes the system design, including the choice of preselection filters, preamplifiers, and RF shielding necessary to measure low RF-noise levels while avoiding intermodulation distortion problems that arise in an environment with many strong emitters. Additionally, we describe techniques developed to reliably geolocate RF data in urban environments. GPS (global positioning system) reception is often poor in dense urban environments. We mitigate this issue by using a 1 m surveying wheel for geolocation.

15. SUBJECT TERMS

Cities and towns, Impulsive, Mapping, Noise, Radio frequency, Radio measurements, Spatial, Thermal noise, Urban, Y-factor

16. SECURITY CLASSIFICATION OF:			**17. LIMITATION OF ABSTRACT**	**18. NUMBER OF PAGES**	**19a. NAME OF RESPONSIBLE PERSON**
a. REPORT Unclassified	**b. ABSTRACT** Unclassified	**c. THIS PAGE** Unclassified	SAR	47	**19b. TELEPHONE NUMBER** *(include area code)*

Standard Form 298 (Rev. 8-98)
Prescribed by ANSI Std. 239.18